Dynamic Nuclear Polarization*

W. A. BARKER

Department of Physics, St. Louis University, St. Louis, Missouri, and Argonne National Laboratory, Lemont, Illinois

I. INTRODUCTION

THE production and detection of nuclear orientation is of interest in several areas of research:

1. The energy and angular distribution of α, β, and γ radiation from oriented radioactive nuclei provides a detailed check on theories of nuclear, weak, and electromagnetic interactions.[1] Similar studies on the angular distribution of decay products from oriented fissionable nuclei are of interest.

2. Adiabatic demagnetization of polarized nuclei extends the range of low temperatures from 10^{-3} °K to 10^{-6} °K.[2]

3. Polarized targets may be used to scatter nuclei, mesons, and hyperons. This is of interest in connection with the spin dependence of nuclear forces and the properties of elementary particles.[3]

4. Simultaneous electron and nuclear spin resonance experiments rearrange the population distributions of the spin systems, thereby providing a sensitive means for obtaining detailed information on the static and dynamic coupling between nuclear spins and their electronic, magnetic, and crystalline environment in gases, liquids, and solids.[4]

5. The sensitivity of nuclear magnetic resonance may be increased by two or three orders of magnitude by dynamic nuclear polarization.[5] This is important in connection with stable isotopes whose natural abundance or gyromagnetic ratio may make detection difficult by standard techniques (e.g., H^2, C^{13}, O^{17}, Ge^{73}).

6. Steady-state inverted-nuclear-spin-population distributions may be used for low-noise quantum-mechanical amplifiers or oscillators in the frequency range from 20 kc/sec to 1000 Mc/sec. Rasers may be of use in radio astronomy or as sensitive magnetometers.[6]

7. The spin population distribution of the host nuclei like Al in the ruby maser may be easily be changed to a considerable extent as a result of the combined action of the microwave pump and the coupling between the nuclear spins and the paramagnetic impurity ions. The gain bandwidth product of a maser can be substantially improved in some instances by depolarizing the nuclei.[7]

The technique of dynamic nuclear orientation as suggested by Overhauser,[8] Jeffries,[9] and Abragam[10] supplement earlier static methods[11] and have been developed to the point where it should now be possible to orient any magnetic nucleus.

If the number of protons or neutrons in a nucleus is odd, the nucleus in the ground state has a nonzero spin and magnetic moment. There are over 130 such magnetic nuclei, about twice as many as the number of nonmagnetic nuclei.

A nucleus of spin I has $2I+1$ spin states denoted by various values of the magnetic quantum number m. Let us suppose that the spin degeneracy is completely lifted by an appropriate field and that N identical nuclei are distributed in some fashion among the allowed levels. If we denote the population of the mth state by n_m with

$$\sum_{m=-I}^{I} n_m = N,$$

the spin system may be completely described by specifying $2I$ n_m values. Alternatively one may define $2I$ orientation parameters which are functions of n_m and I.

* Supported by the Atomic Energy Commission and the Air Force Office of Scientific Research.

[1] R. J. Blin-Stoyle, M. A. Grace, and H. Halban, *Progress in Nuclear Physics* (Pergamon Press, New York, 1957), Vol. 3; M. J. Steenland and H. A. Tolhoek, *Progress in Low-Temperature Physics* (Pergamon Press, New York, 1959), Vol. 7.

[2] N. Kurti, F. N. H. Robinson, F. Simon, and D. A. Spohr, Nature **178**, 450 (1956); C. D. Jeffries, *Progress in Cryogenics* (Heywood and Co., London, 1961), p. 169.

[3] R. H. Capps, Phys. Rev. Letters **3**, 202 (1959); C. Hwang and T. M. Sanders, Jr., *Proceedings of 7th International Conference on Low-Temperature Physics*, edited by G. M. Graham and A. C. H. Hewlett (University of Toronto Press, Toronto, 1961), Chap. 7.

[4] An excellent review is given by R. H. Webb, Am. J. Phys. **29**, 428 (1961).

[5] This was reviewed in an invited paper by W. A. Barker presented at the American Chemical Society's Chicago meeting in September 1961. The experimental work of J. Combrisson, J. phys. radium **19**, 840 (1958) on H^2; and of D. J. Parker, G. A. McClaren, and J. J. Conradi on C^{13} [J. Chem. Phys. **33**, 629 (1960)] are interesting cases in point.

[6] W. A. Barker and E. A. Desloge, Bull. Am. Phys. Soc. **2**, 226 (1957); Mohan Lal Narchal and W. A. Barker, *ibid.* **6**, 298 (1961); E. Allais, Compt. rend. **246**, 2123 (1958); I. Solomon, J. phys. radium **19**, 837 (1958).

[7] J. A. Cowen, W. R. Schafer, and R. D. Spence, Phys. Rev. Letters **3**, 13 (1959); G. Mahkov, L. G. Cross, R. W. Terhune, and J. Lambe, J. Appl. Phys. **31**, 936 (1960); R. W. Terhune, J. Lambe, G. Mahkov, and L. G. Cross Phys. Rev. Letters **4**, 234 (1960).

[8] A. W. Overhauser, Phys. Rev. **89**, 689 (1953); **92**, 411 (1953).

[9] C. D. Jeffries, Phys. Rev. **106**, 164 (1957).

[10] A. Abragam and W. G. Procter, Compt. rend. **246**, 2253 (1958).

[11] C. J. Gorter, Physica **14**, 504 (1948); M. E. Rose, Phys. Rev. **75**, 213 (1949); J. W. T. Dabbs, L. D. Roberts, and S. Bernstein, *ibid.* **98**, 1512 (1955).

The first such parameter is the nuclear polarization

$$P_N \equiv f_1 \equiv \frac{\sum_m m n_m}{I \sum_m n_m}. \quad (1)$$

In this paper, we restrict attention primarily to $I=\frac{1}{2}$ and consequently do not discuss in detail the nuclear alignment

$$f_2 \equiv \frac{1}{(2I-1)I}\left\{\frac{3\sum_m m^2 n_m}{\sum_m n_m} - I(I+1)\right\} \quad (2)$$

or orientation parameters of higher order.

In the accompanying nuclear polarization chart, the energy level scheme, population distribution, enhancement of the nuclear magnetic resonance, nuclear polarization, and electronic polarization are tabulated for 4 static and 24 dynamic cases.

In Sec. II, the construction of the nuclear polarization chart is described in detail; in Sec. III, the utility and significance of the chart is discussed.

II. NUCLEAR POLARIZATION CHART

A. Spin Hamiltonian

All of the results tabulated in the chart are a consequence of the spin Hamiltonian

$$\mathcal{H} = -g\beta \mathbf{S}\cdot\mathbf{H} - g_n\beta_n \mathbf{I}\cdot\mathbf{H} + \mathbf{I}\cdot\mathbf{A}\cdot\mathbf{S}, \quad (3)$$

where g is the electron g value; $\beta = e\hbar/2mc$ is the electron Bohr magneton; $\mathbf{S}$ is the electron spin operator; $\mathbf{A}$ is the hyperfine structure tensor; $\mathbf{H}$ is the external and local magnetic field; g_n is the nuclear g value; $\beta_n = e\hbar/2Mc$ is the nuclear Bohr magneton; $\mathbf{I}$ is the nuclear spin operator. All vector and tensor components in the spin Hamiltonian may have time varying as well as static elements. Crystal field and nuclear quadrupole interactions are not included in $\mathcal{H}$.

B. Eigenvalue Equation

If the electron Zeeman energy is large compared to both the nuclear Zeeman energy and the hyperfine interaction energy and if anisotropic effects are neglected, the eigenvalue equation is

$$E(M,m) = -g\beta H_0 M - g_N\beta_N H_0 m + AMm, \quad (4)$$

where H_0 is the external static magnetic field and M and m are the magnetic quantum numbers of the electron and nucleus, respectively. A word about algebraic signs is in order: The electronic gyromagnetic ratio $\gamma_e \equiv \beta/\frac{1}{2}\hbar$ is negative, so we take β negative. The nuclear gyromagnetic ratio $\gamma_n \equiv \mu_n/I\hbar = g_n\beta_n/\hbar$ may be either positive or negative. We take β_n positive and denote the sign of γ_n or of the nuclear magnetic moment μ_n by specifying a positive or negative g_n value. The hyperfine constant A may be either positive or negative. Its sign is not necessarily the same as that of γ_n.[12] For simplicity, I and S are both taken equal to $\frac{1}{2}$. Consequently all 28 energy-level diagrams in the chart have 4 levels. Two limiting cases are treated: nuclear Zeeman energy large or small compared to the hyperfine structure energy. Thus

$$E(M,m) = -g\beta H_0 M - g_N\beta_N H_0 m \quad \text{when} \quad |g_N\beta_N H_0| \gg |A| \quad (4a)$$

or

$$E(M,m) = -g\beta H_0 M + AMm \quad \text{when} \quad |A| \gg |g_N\beta_N H_0|. \quad (4b)$$

The designation of quantum states in Figs. 1 and 2 of the Nuclear Polarization chart is a consequence of Eq. (4a) for $\gamma_n > 0$ and $\gamma_n < 0$, respectively. The description of quantum states in Figs. 3 and 4 is a consequence of Eq. (4b) for $A>0$ and $A<0$, respectively. These exemplify the only four possible ways in which the levels may be labeled. See the chart at the end of this paper.

C. Population Distribution

The population distribution among the 4 energy levels for any one of the 4-possible energy-level diagrams depends on (1) the magnitude and orientation of the pumping radiation, (2) the nature of the coupling between the electron and nuclear spin systems, and (3) the type and relative magnitude of the relaxation mechanisms.

If there is no pumping radiation at all the population distribution is a Boltzmann distribution as indicated in the "brute force" and Rose-Gorter cases (Figs. 1–4). Here (and elsewhere in the chart) only relative (unnormalized populations) are tabulated and the linear approximation to the exponential is employed on the assumption that $\Delta \equiv E_3 - E_1/kT \ll 1$ and $\delta \equiv E_2 - E_1/kT \ll 1$.

If the pumping radiation is such as to induce an allowed transition $\Delta M = \pm 1$, $\Delta m = 0$, then we obtain an Overhauser effect. This is illustrated in Figs. 5–20. The pumping radiation is usually provided by a time varying field oriented at right angles to the dc magnetic field H_0. A saturation of 100% is assumed in the chart.

If the pumping radiation induces a "forbidden" transition $\Delta M = \pm 1$, $\Delta m = \mp 1$, or $\Delta M = \pm 1$, $\Delta m = \pm 1$, then we have a Jeffries-Abragam effect.[13] This is illus-

[12] A. Abragam and M. H. L. Pryce, Proc. Roy. Soc. (London) **A205**, 135 (1951); For example Mn^{55} has a positive γ_n, but in the deuterated paramagnetic salt $Mn^{55}SO_4 \cdot (ND_4)_2 \cdot 6D_2O$ the hyperfine constant A is negative. S. Bernstein, L. D. Roberts, C. P. Stanford, J. W. T. Dabbs, and T. E. Stephenson, Phys. Rev. **94**, 1243 (1954).

[13] In reference 4, Webb distinguishes between the "Jeffries effect" and the "solid effect" of Abragam and Procter. Both are

trated in Figs. 21–28. The static coupling $\mathbf{I}\cdot\mathbf{A}_0\cdot\mathbf{S}$ between the nuclear and electron spin provides an admixture of states which permits such transitions to take place. The pumping radiation is applied by a linear time varying magnetic field with an orientation sometimes taken as perpendicular and sometimes parallel to the static field. Complete saturation of the "forbidden" transition is assumed.

In the presence of saturating radiation, the resulting steady-state population distribution is non-Boltzmann and is determined by 4 different relaxation mechanisms: (1) R_e: electron paramagnetic relaxation $\Delta M=\pm 1$, $\Delta m=0$; (2), (3) R_{en}: cross relaxations[14] of the flip-flop ($\Delta M=\pm 1$, $\Delta m=\mp 1$) or flip-flip ($\Delta M=\pm 1$, $\Delta m=\pm 1$) variety; and (4) R_n: nuclear paramagnetic relaxation $\Delta M=0$, $\Delta m=\pm 1$. In this treatment R_n is neglected as it is usually much smaller than R_{en} or R_e. All 24 cases of dynamic polarization (Figs. 5–28) are treated by choosing a minimum number of noncompeting dominant relaxations. These are the "pure" cases.

As a typical example, consider the situation depicted in Fig. 5. Here there are two pumps and one relaxation connecting the four levels. The steady-state solution to the rate equations determines the relative population distribution n_i: $i=1,2,3,4$.

$$\begin{aligned} dn_1/dt&=-n_1W_{13}+n_3W_{31}-n_1w_{14}+n_4w_{41}=0\\ dn_2/dt&=-n_2W_{24}+n_4W_{42}=0\\ dn_3/dt&=-n_3W_{31}+n_1W_{13}=0\\ dn_4/dt&=-n_4W_{42}+n_2W_{24}-n_4w_{41}+n_1w_{14}=0. \end{aligned} \tag{5}$$

The W_{ij} are radiative induced transition probabilities with $W_{ij}=W_{ji}$ by virtue of the Hermiticity of the relevant quantum mechanical operators. Further $W_{13}=W_{24}$ inasmuch as both transitions are of precisely the same character (i.e., $\Delta M=\pm 1$, $\Delta m=0$). The w_{ij} are thermal transition probabilities with $w_{ij}=w_{ji}e^{(E_i-E_j)/kT}$. Only three of these four rate equations are independent. It is clear from Eqs. (5) that

$$\frac{n_1}{n_3}=\frac{n_2}{n_4}=1 \quad \text{and} \quad \frac{n_4}{n_1}=\frac{w_{14}}{w_{41}}=e^{-\Delta-\delta}\simeq 1-\Delta-\delta, \tag{6}$$

from which n_1 and n_3 may be taken as unity, and n_2 and n_4 as $1-\Delta-\delta$. The relative population distribution for all the remaining cases of dynamic polarization may be obtained either by solving the relevant rate equations or by inspection, making use of the simple rule that pumps are equalizers and relaxations are thermalizers.

D. Enhancement, Nuclear Polarization, Electronic Polarization

The enhancement of the nuclear magnetic resonance signal, $\mathcal{E}$; the nuclear polarization, P_N; and the electronic polarization P_e may now be readily calculated as functions of Δ and δ alone, using the definitions of these quantities and the unnormalized population distribution.

The enhancement may be defined as the power absorbed by the nuclear spin system in the presence of saturating radiation divided by the power absorbed by the nuclear spin system in the absence of saturating radiation.

$$\mathcal{E}\equiv\frac{P_s}{P_0}=\frac{(n_1-n_2)h\nu_{12}W_{12}+(n_3-n_4)h\nu_{43}W_{43}}{(n_1^0-n_2^0)h\nu_{12}W_{12}+(n_3^0-n_4^0)h\nu_{43}W_{43}}, \tag{7}$$

where n_i^0 denotes the relative Boltzmann population distribution for the ith level. Using $h\nu_{12}=h\nu_{43}=\delta kT$, $W_{12}=W_{34}$ and the linear approximation to the Boltzmann factor, the enhancement reduces to

$$\mathcal{E}\simeq\frac{(n_1+n_3)-(n_2+n_4)}{2\delta}=\mathcal{E}(\Delta,\delta). \tag{8}$$

The nuclear polarization for $I=\frac{1}{2}$ may be obtained directly from Eq. (1). In terms of the unnormalized n_i:

$$P_N=2\sum_{i=1}^{4}n_im_i/\sum_{i=1}^{4}n_i=P_N(\Delta,\delta). \tag{9}$$

Similarly, the electronic polarization for $S=\frac{1}{2}$ may be written

$$P_e=2\sum^{4}n_iM_i/\sum_{i=1}^{4}n_i=P_e(\Delta,\delta). \tag{10}$$

III. DISCUSSION

The nuclear polarization chart may be used to provide a preliminary understanding of experiments which have been performed or are being contemplated. It also serves as a convenient means for comparing a number of the principal features of the various polarization methods. A full understanding of a given experiment or method requires consideration of such complicating effects as the nonlinear terms in the Boltzmann factor, partial saturation by the pumping or detection field, competition among relaxation mechanisms or among radiative induced transitions, and nuclear spin greater than one half. All of these effects were neglected in the preparation of the chart.

---

associated with forbidden transitions. In the Jeffries effect the pump field is applied parallel to H_0 and scalar coupling between I and S mixes the states so that a flip-flop ($\Delta M=\pm 1$, $\Delta m=\mp 1$) radiative transition may be induced. In the "solid effect" the pump field is applied perpendicular to H_0 and a tensor coupling between $\mathbf{I}$ and $\mathbf{S}$ admixes the states so that a flip-flip ($\Delta M=\pm 1$, $\Delta m=\pm 1$) radiative transition may be induced.

[14] In this context, cross relaxation refers to simultaneous electron and nuclear spin flips. Cf. N. Bloembergen, S. Shapiro, P. S. Pershan, and J. O. Artman, Phys. Rev. **114**, 445 (1959).

A. Experimental Results

In 1953–4 the first two successful dynamic nuclear polarization experiments were reported: Carver and Slichter[15] polarized the Li^7 nucleus in metallic lithium. Beljers, van der Kint and Wieringen[16] polarized the H^1 nucleus in the solid DPPH free radical. The detection of the nuclear polarization in these two experiments was by the enhancement of the NMR signal.

From 1956–61 more than a dozen different nuclei have been dynamically polarized in a rich variety of paramagnetic materials. The experiments have been performed using fields ranging from ~ 1 to 13 000 gauss and temperatures from 1° to 350°K. Three different detection methods have been used.

In Table I, the experimental results are summarized and keyed to the nuclear polarization chart. In columns 1 and 2 the nucleus polarized and its paramagnetic environment is described. In columns 3 and 4 the static external field and temperature are tabulated. In column 5 the observed enhancement of the NMR signal is given unless one of the other two detection methods is specifically indicated. In column 6 reference is made to a figure in the nuclear polarization chart which best describes the experiment. If the effect was produced by saturation of an allowed or forbidden transition this is denoted by (A) or (F) in column 6. In the last column the appropriate reference to the published literature is cited.

Dynamic nuclear orientation is possible by virtue of the coupling between the nuclear spin and an unpaired electron spin. The paramagnetic environment may be provided by (1) the conduction electrons in metals or metal ammonia solutions, (2) the donor or acceptor electrons in semi-conductors, (3) paramagnetic ions in a diamagnetic solid (4) paramagnetic ions in solution, (5) free radicals, and (6) color centers.

Detection of dynamic nuclear orientation may be achieved by at least three different methods: (1) enhancement of the NMR signal, (2) the shift in the EPR frequency, and (3) the β asymmetry or γ anisotropy from an oriented radioisotope.

The most commonly used detection technique is to observe the enhancement of the NMR signal. This may be readily done at room temperatures when the nuclear polarization or alignment is very small. If the nuclear spin lattice relaxation time is of the order of seconds or less, then the production and detection of nuclear polarization involves observation of an NMR signal at the same time that an EPR line in the sample is being saturated. On the other hand if the nuclear T_1 is of the order of minutes or longer, the production of nuclear polarization and its detection may be separated in time and in space.[17]

In metals and possibly in semiconductors, the nuclear polarization may be detected at tempeuatures $\sim$ 1°K by the shift in the EPR resonance. This was first pointed out by Overhauser[8] after whom the shift was named. A successful Overhauser-shift measurement has recently been reported in metallic lithium by Ryter.[18]

In the case of the radio isotopes, their abundance in a given sample is usually so small that detection by the enhancement of the NMR or by a shift in the EPR is not possible. However the angular distribution of the decay products does depend on the orientation of the nuclei and this provides an extremely sensitive detection technique.[19] Application of a strong rf signal at the Larmor frequency of the nucleus should quench the orientation and the resulting β asymmetry or γ anisotropy. Hence double resonance may be used to determine an unknown nuclear magnetic moment as demonstrated by Connor[20] in his work on Li^8 and F^{20}.

B. Comparison of Polarization Methods

1. Energy-level splittings

In all 28 figures of the nuclear polarization chart, the electronic Zeeman splitting is given by

$$E_3-E_1=E_4-E_2=\Delta kT=g\beta H_0=|\gamma_e|\hbar H_0. \quad (11)$$

This amounts to 10 000 Mc/sec in a field of 3600 gauss for $g=2$. The nuclear-energy level splitting

$$E_2-E_1=E_4-E_3=\delta kT \quad (12)$$

depends on the relative magnitude of the nuclear Zeeman interaction and the hyperfine interaction. If the former dominates then

$$\delta kT=|g_N|\beta_N H_0=|\gamma_n|\hbar H_0. \quad (13)$$

But if the latter dominates then

$$\delta kT=|A|/2. \quad (14)$$

The nuclear Zeeman splitting in a field of 3600 gauss ranges from a fraction of megacycle/second to 15 Mc/sec depending on the magnitude of γ_n. The nuclear hyperfine splitting has a much greater range attaining values up to 1000 Mc/sec for large A. The energy level splittings determine the pump and signal frequencies.

---

[15] T. R. Carver and C. P. Slichter, Phys. Rev. **92**, 212 (1953).
[16] H. G. Beljers, L. Van der Kint, and J. J. Wieringen, Phys. Rev. **95**, 1683 (1954).
[17] A. Abragam, A. Landesman, and J. M. Winter, Compt. rend. **247**, 1852 (1958).
[18] Ch. Ryter, Phys. Rev. Letters **5**, 10 (1960). [A similar shift has been observed in metallic sodium, W. Gager (private communication).]
[19] C. S. Wu, E. Ambler, R. W. Hayward, D. D. Hoppes, and R. P. Hudson, Phys. Rev. **105**, 1413 (1957).
[20] D. Connor, Phys. Rev. Letters **3**, 429 (1959). Tung Sang and D. Connor, Bull. Am. Phys. Soc. **7**, 292 (1962).

Thus

$$\begin{aligned} f_P &= |\gamma_e| H_0/2\pi \quad \text{(Figs. 5–8, 25–28)} \\ f_P &= |\gamma_e| H_0/2\pi \pm A/2h \quad \text{(Figs. 9–20)} \\ f_P &= (|\gamma_e| \pm \gamma_n) H_0/2\pi \quad \text{(Figs. 21–24)} \end{aligned} \tag{15}$$

and

$$\begin{aligned} f_S &= |\gamma_n| H_0/2\pi \quad \text{(Figs. 5–8, 21–24)} \\ f_S &= A/2h \quad \text{(Figs. 9–20, 25–28).} \end{aligned} \tag{16}$$

2. Enhancement

(a) $\mathcal{E}=1$ for all static cases (Figs. 1–4) by definition. It is also unity for the Jeffries-Abragam effect when the hyperfine interaction is large in comparison with the nuclear Zeeman energy (Figs. 25–28).

(b) $\mathcal{E}=0$ for four cases of the Overhauser effect when the hyperfine interaction is large in comparison with the nuclear Zeeman energy and 2 paramagnetic pumps are used. (Figs. 17–20). It is clear from the diagrams that the population distribution for one pair of nuclear levels is inverted but for the second pair the population distribution is normal. Stimulated emission from the inverted pair will be compensated by absorption from the normal pair. This result may occur in a practical situation when the linewidth of the saturating field is greater than the nuclear splitting: $\Delta H \geq |A|/2|\gamma_e|\hbar$.

(c) The possibility of small $\mathcal{E}$ may occur when there are two almost equal competing relaxation mechanisms where one tends to produce a positive $\mathcal{E}$ and the other a negative $\mathcal{E}$ (e.g., Figs. 5 and 7). A comparable cancellation can occur when there are two competing pumps or one pump in which the linewidth $\Delta H \geq (|\gamma_n|/|\gamma_e|)H_0$ (e.g., Figs. 21 and 23).

(d) $\mathcal{E}<0$ for six Overhauser effect cases and two Jeffries-Abragam effect cases (Figs. 6, 7, 9–12, 21, and 22).

$$\begin{aligned} \mathcal{E}_{6,7} &= -(|\gamma_e| - |\gamma_n|)/|\gamma_n| \\ \mathcal{E}_{21,22} &= -|\gamma_e|/|\gamma_n| \\ \mathcal{E}_{9,10,11,12} &= -(|\gamma_e|\hbar H_0 - |A|/2)/|A| \end{aligned} \tag{17}$$

These eight cases are all favorable for Raser action.

(e) $\mathcal{E} \gg 1$ for six Overhauser-effect cases and two Jeffries-Abragam effect cases. (Figs. 5, 8, 13–16, 23, 24).

$$\begin{aligned} \mathcal{E}_{5,8} &= (|\gamma_e| + |\gamma_n|)/|\gamma_n| \\ \mathcal{E}_{23,24} &= |\gamma_e|/|\gamma_n| \\ \mathcal{E}_{13,14,15,16} &= (|\gamma_e|\hbar H_0 + |A|/2)/|A|. \end{aligned} \tag{18}$$

All 16 cases of large $|\mathcal{E}|$ represented by Eqs. (17) and (18) are favorable for increasing the sensitivity of an NMR signal. The numerical value of this enhancement is given to a good approximation by

$$|\mathcal{E}|_{\text{optimum}} \simeq f_P/f_S \tag{19}$$

and may range from 10 to 10^5.

3. Nuclear Polarization

Among the static methods of nuclear polarization the Rose-Gorter method[21] (Figs. 3–4) is clearly more favorable than the brute force method[22] (Figs. 1–2):

$$\frac{P_N(\text{R.G.})}{P_N(\text{B.F.})} = \frac{|\gamma_e|}{4kT}\frac{|A|}{|\gamma_n|}. \tag{20}$$

All 24 dynamic cases have a nuclear polarization value whose magnitude is about the same:

$$P_N \approx \Delta/2 = |\gamma_e|\hbar H_0/2kT. \tag{21}$$

In principle, dynamic nuclear poarization should yield higher values of P_N than the Rose-Gorter method:

$$\frac{P_N(\text{dynamic})}{P_N(\text{R-G})} \simeq \frac{4kT}{|A|}. \tag{22}$$

In practise the 60% nuclear polarization achieved by Wu *et al.*[19] by the Rose-Gorter method has not as yet been surpassed in a dynamic nuclear polarization experiment. The recent impressive work of Leifson and Jeffries[23] indicates, however, that nuclear polarization values in excess of 25% may soon be obtained by dynamic methods.

In the Overhauser effect, the best values of nuclear polarization are obtained when the electronic polarization is reduced to zero. If all the paramagnetic ($\Delta M = \pm 1$, $\Delta m = 0$) transitions are not completely saturated as in cases 9–16, the resulting $P_N \simeq |\gamma_e|\hbar H_0/4kT$ which is about one half of the optimum value.

A large nuclear polarization is not necessarily accompanied by a large enhancement of the NMR signal. This is illustrated both by the Overhauser effect and by the Jeffries-Abragam effect. In Figs. 17–20 and again in Figs. 25–28 $|P_N| = |\gamma_e|\hbar H_0/2kT$, but $\mathcal{E}=0$ in the Overhauser effect cases cited and $\mathcal{E}=1$ in the Jeffries-Abragam effect cases cited. This is a rather interesting point because it indicates that the failure of a nuclear polarization experiment cannot be based entirely on small observed $\mathcal{E}$ values.

The algebraic sign of P_N may be + or − and is not related in any simple way to the sign of $\mathcal{E}$. $P_N<0$ means simply that the nuclear polarization is anti parallel to the applied external field. In the event γ_n and P_N have opposite signs, the nuclear magnetization

$$M_N = \gamma_n \hbar I P_N < 0 \quad \text{(e.g., Figs. 6 and 7)} \tag{23}$$

This has the effect of shifting the electron spin resonance frequency to a value less than $f_e = |\gamma_e| H_0/2$.

[21] C. J. Gorter, Physica **14**, 504 (1948); M. E. Rose, Phys. Rev. **75**, 213 (1949); A. Simon, M. E. Rose, and J. M. Jauch, *ibid.* **84**, 1155 (1951); E. Ambler, M. A. Grace, H. Halban, N. Kurti, H. Durand, C. E. Johnson, and H. R. Lemmer, Phil. Mag. **44**, 216 (1953); S. Bernstein, L. D. Roberts, C. P. Stanford, J. W. T. Dabbs and T. E. Stephenson, Phys. Rev. **94**, 1243 (1954); and C. S. Wu, E. Ambler, R. W. Hayward, D. D. Hoppes, and R. P. Hudson, *ibid.* **105**, 1413 (1957).

[22] J. W. T. Dabbs, L. D. Roberts, and S. Bernstein, Phys. Rev. **98**, 1512 (1955).

[23] O. S. Leifson and C. D. Jeffries, Phys. Rev. **122**, 1781 (1961).

4. *Electronic Polarization*

In the Overhauser effect, the electronic rpolaization is completely or partially removed by the pump field. In the Jeffries-Abragam effect the electronic polarization remains unchanged from its static value.

$$P_e \simeq \gamma_e \hbar H_0 / 2kT \tag{24}$$

This is one of the most significant differences in the two methods of producing a non-Boltzmann nuclear polarization. In metals and semiconductors the Overhauser effect should be accompanied by a decrease in the observed NMR frequency. In fact this quenching of the Knight shift may be used to determine the degree of saturation of the EPR as pointed out by Barker and Mencher[24]:

$$s = \frac{H_0 - 2\pi f_s/\gamma_n}{\Delta H} + 1. \tag{25}$$

Here s is the saturation parameter as defined by Overhauser,[8] ΔH is the Knight shift observed in the absence of an EPR pump field, and f_s is the NMR frequency observed in the presence of the pump field.

ACKNOWLEDGMENTS

The author expresses gratitude to the Solid-State Science Division of the Argonne National Laboratory for hospitality during the summer of 1960 when a large portion of this work was carried out. The encouragement and comments of Dr. B. Smaller of Argonne and of Dr. D. P. Ames of the McDonnell Aircraft Company are much appreciated. Correspondence with Dr. C. D. Jeffries and Dr. P. Scott of the University of California has been most helpful. Miss C. Birkbeck's careful review of the manuscript is gratefully acknowledged.

[24] W. A. Barker and A. Mencher, Phys. Rev. **98**, 1868 (1955).

TABLE I. Experimental results.

Nucleus polarized	Paramagnetic environment	H_0(gauss)	T(°K)	Observed enhancement of NMR signal	Nuclear polarization chart (A) indicates allowed transitions (F) indicates forbidden transitions	Reference
H^1	Conduction electrons in Na metal in liquid NH_3	11.7	300	480	Fig. 5 (A)	c
H^1	Ionic free radical Na and napththelene in 1,2 dimethoxyethane	17.8	300	−65	Fig. 7 (A)	d
H^1	Solid DPPH free radical $(C_6H_5)_2N\text{-}NC_6H_2(NO_2)_3$	3300	300	9	Fig. 5 (A)	e
H^1	Solution of disulfonate of peroxylamine $(SO_3)_2NOK_2$	3000	300	−40	Fig. 7 (A)	f
		0.5	300	−3880	Fig. 11 (A)	
H^1	Finely divided DPPH in propane gas	42.3	300	−7	Fig. 7 (A)	g
H^1	Free radical asphaltine in crude oil	18.5	300	−15	Fig. 7 (A)	h
H^1	Roofing tar (asphaltine) dissolved in benzene or xylene	18.6	300	−35	Fig. 7 (A)	i
H^1	Protons in H_2O adsorbed on charred (paramagnetic) sucrose	3600	300	+16	Fig. 23 (F)	j
				−16	Fig. 21 (F)	
H^1	Protons in radiation damaged polyethylene	3500	1.2,2.1,77	+40	Fig. 23 (F)	k
				−40	Fig. 21 (F)	
H^1	Protons in interior of paramagnetic carbon	3240	300	150	Fig. 5 (A)	l
H^1	Protons in benzene, toluene ammonia and H_2S adsorbed on amorphous carbon	3000	300	+20	Fig. 23 (F)	m
				−20		
H^1	Mn^{++} in aqueous solution of $MnCl_2$	5,10,18	300	300	Fig. 5 (A)	n
H^1	Ce^{3+} in $Ce_2Mg_3(NO_3)_6 \cdot 24H_2O$	3300	1.2–1.6	+25	Fig. 23 (F)	o
				−25	Fig. 21 (F)	o
H^1	5% Ce^{3+} in $La_2Mg_3(NO_3)_6 \cdot 24H_2O$	3300	1.2–1.6	+60,150	Fig. 23 (F)	o,p
				−60,150	Fig. 21 (F)	
H^2	10^{-2} molar solution of $NO(SO_3)_2K_2$	3000	300	a	Fig. 7 (A)	q
Li^7	Conduction electrons in Li metal	30.3	343	110	Fig. 5 (A)	r
Li^7	F centers in LiF produced by x radiation	3300	1.2–1.6	+17	Fig. 23 (F)	o
Li^7	F centers in LiF	13 000	1.2–1.6	+58	Fig. 23 (F)	o
				−58	Fig. 21 (F)	
Li^7	Colloidal metallic Li in paraffin	41	343	8	Fig. 5 (A)	s
Li^7	Colloidal metallic Li in oil	30.1	77.2–373	...	Fig. 5 (A)	t
Li^7	Colloidal particles of metallic Li produced by irradiating LiH with neutrons or ultraviolet	3300	300	100	Fig. 5 (A)	u
		3300	4.2	Detection by Overhauser shift	Fig. 5 (A)	v

TABLE I (*continued*)

Nucleus polarized	Paramagnetic environment	H_0(gauss)	T(°K)	Observed enhancement of NMR signal	Nuclear polarization chart (A) indicates allowed transitions (F) indicates forbidden transitions	Reference
C^{13}	Conduction electrons in graphite	3240[b] 2.7	300	300	Fig. 5 (A)	w
C^{13}	Solutions of 2, 6, 3′, 5′ tetra tert butyl 4 phenoxy 4 methylene-2, 5 hexadrene-1-one radical, *I*, in toluene	3300	300	a	Fig. 7 (A)	q
F^{19}	$C_6H_4(CF_3)_2$ in $NO(SO_3)_2K_2$	100	300	−35	Fig. 7 (A)	y
F^{19}	0.01% Ce^{3+} in CaF_2	3300	1.2–1.6	+2 −2	Fig. 23 (F) Fig. 21 (F)	o
F^{19}	*F* centers in LiF produced by x rays	3300	1.2–1.6	+17 −17	Fig. 23 (F) Fig. 21 (F)	o
F^{19}	Paramagnetic centers produced by electron bombardment of polyetrafluorethylene	3300	1.2–1.6	+38 −38	Fig. 23 (F) Fig. 21 (F)	o
Na^{23}	Conduction electrons in Na metal	44.2	320	10	Fig. 5 (A)	c
Al^{27}	0.1% Cr^{3+} in Al_2O_3	3300	1.2–1.6	+5 −5	Fig. 23 (F) Fig. 21 (F)	o
Si^{29}	Donor electrons in phosphorus doped Si	3300	77	−100	Fig. 6 (A)	
Si^{29}	5×10^{16} donor electrons in phorphorus doped Si	3300	4.2	−30	Fig. 22 (F)	y
$Mn^{52,54}$	Mn^{++} in $La_2Mg_3(NO_3)_{12}\cdot24H_2O$	3000	1.5	Detection by γ-ray anisotropy	Fig. 9 (A) Fig. 25 (F) Fig. 27 (F)	z
Co^{59}	2.5% Fe^{++} in $K_3Co(CN)_6$	3300	1.2–1.6	+2 −2	Fig. 23 (F) Fig. 21 (F)	o
Co^{60}	Co^{++} in $La_2Mg_3(NO_3)_{12}\cdot24D_2O$	1500	1.5	Detection by γ-ray anisotropy	Fig. 9 (A) Fig. 25 (F)	aa
As^{76}	As donor electrons in doped Si crystal	8350	1.25	Detection by γ-ray anisotropy	Fig. 26 (F)	bb
Sb^{122}	Sb donor electrons in doped Si crystal	8500	1.25	Detection by γ-ray anisotropy	Fig. 26 (F) Fig. 14 (A)	cc

[a] In the absence of the pump field the NMR was unobservable because the signal was lost in noise.
[b] Longitudinal relaxation time of the C^{13} nucleus ~ minutes. Hence the production of polarization and its detection by adiabatic fast passage were separated in time and space.
[c] T. R. Carver and C. P. Slichter, Phys. Rev. **92**, 212 (1953); **102**, 975 (1956).
[d] L. H. Bennett and H. C. Torrey, Phys. Rev. **108**, 499 (1957).
[e] Reference 16.
[f] A. Abragam, J. Combrisson and I. Solomon, Compt. rend. **245**, 157 (1957); E. Allais, *ibid.* **246**, 2123 (1958); I. Solomon, J. Phys. radium **19**, 837 (1958).
[g] J. P. Borel and P. Cornaz, Compt. rend. **247**, 1988 (1958).
[h] E. H. Poindexter, Nature **182**, 1087 (1958).
[i] E. H. Poindexter, J. Chem. Phys. **31**, 1477 (1959).
[j] J. Krebs, J. Chem. Phys. **34**, 326 (1961).
[k] Reference 3.
[l] A. Abragam, A. Landesman, and J. M. Winter, Compt. rend. **247**, 1852 (1958).
[m] E. Erb, J. L. Motchane, and J. Uebersfeld, Compt. rend. **246**, 2121 (1958); **246**, 3050 (1958); J. Phys. radium **19**, 843 (1958).
[n] R. S. Codrington and N. Bloembergen, J. Chem. Phys. **29**, 601 (1958).
[o] M. Abraham, M. A. H. McCausland, and F. N. H. Robinson, Phys. Rev. Letters **2**, 449 (1959).
[p] Reference 23.
[q] Reference 5.
[r] Reference 15.
[s] C. Manus and J. P. Borel, Helv. Phys. Acta **29**, 249 (1956).
[t] N. A. Bekeshko and E. L. Kondorskii, Soviet Phys.—JETP **5**, 505 (1957).
[u] M. Gueron and Ch. Ryter, Phys. Rev. Letters **3**, 338 (1958).
[v] Reference 18.
[w] Reference 17.
[x] A. Abragam, J. Combrisson, and I. Solomon, Compt. rend. **246**, 1035 (1958).
[y] A. Abragam, J. Combrisson, and I. Solomon, Compt. rend. **247**, 2337 (1958); J. Combrisson and I. Solomon, J. Phys. radium **20**, 683 (1959).
[z] R. W. Kedzie, M. Abraham, C. D. Jeffries, and O. Leifson, Bull. Amer. Phys. Soc. **2**, 382 (1957); R. W. Kedzie and C. D. Jeffries Bull. *ibid.* **3**, 415 (1958).
[aa] M. Abraham, R. W. Kedzie, and C. D. Jeffries, Phys. Rev. **106**, 165 (1957); **117**, 1070 (1960).
[bb] F. M. Pipkin and J. W. Culvahouse, Phys. Rev. **109**, 1423 (1958).
[cc] F. M. Pipkin, Phys. Rev. **112**, 935 (1958).

NUCLEAR POLARIZATION CHART

ARGONNE NATIONAL LABORATORY
Prepared by: William A. Barker
August 1960

SYMBOLS

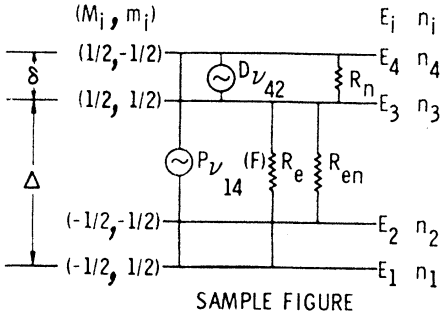

SAMPLE FIGURE

$\delta, \Delta << 1$ ENERGY SPACINGS IN UNITS OF kT.

$\delta = (E_2-E_1)/kT = (E_4-E_3)/kT = h\nu_{21}/kT = h\nu_{43}/kT.$

$\Delta = (E_4-E_2)/kT = (E_3-E_1)/kT = h\nu_{42}/kT = h\nu_{31}/kT.$

M_i = ELECTRONIC MAGNETIC QUANTUM NUMBER FOR ith LEVEL.

m_i = NUCLEAR MAGNETIC QUANTUM NUMBER FOR ith LEVEL.

E_i = ENERGY OF ith LEVEL.

n_i = RELATIVE (UNNORMALIZED) POPULATION OF ith LEVEL.

N = TOTAL NUMBER OF SPINS.

γ_n = NUCLEAR GYROMAGNETIC RATIO.

A = HYPERFINE STRUCTURE CONSTANT.

$\mathcal{E}$ = ENHANCEMENT OF NUCLEAR MAGNETIC RESONANCE.

P_ν PUMPING BY EXTERNAL r f FIELD AT FREQUENCY ν.

$P_\nu(A)$ PUMPING OF ALLOWED TRANSITIONS: $\Delta M = \pm 1, \Delta m = 0$.

$P_\nu(F)$ PUMPING OF "FORBIDDEN" TRANSITIONS: $\Delta M = \pm 1, \Delta m = \mp 1$ OR $\Delta M = \pm 1, \Delta m = \pm 1$.

D_ν DETECTION BY EXTERNAL r f FIELD AT FREQUENCY ν.

R_e PARAMAGNETIC RELAXATION: $\Delta M = \pm 1, \Delta m = 0$.

R_{en} CROSS RELAXATION: $\Delta M = \pm 1, \Delta m = \mp 1$ (FLIP-FLOP) OR $\Delta M = \pm 1, \Delta m = \pm 1$ (FLIP-FLIP).

R_n NUCLEAR RELAXATION: $\Delta M = 0, \Delta m = \pm 1$.

a + (-) SIGN FOR P_N OR P_e MEANS THAT THE NUCLEAR OR ELECTRONIC POLARIZATION IS PARALLEL (ANTI-PARALLEL) TO THE APPLIED EXTERNAL FIELD.

$$P_N \equiv \frac{2\sum_i n_i m_i}{\sum_i n_i} = \text{NUCLEAR POLARIZATION.}$$

$$P_e \equiv \frac{2\sum_i n_i M_i}{\sum_i n_i} = \text{ELECTRONIC POLARIZATION.}$$

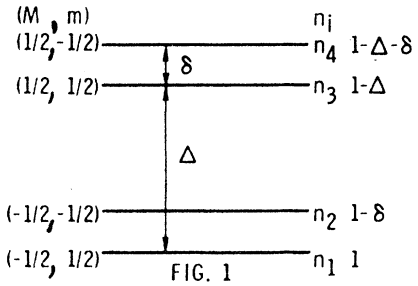

FIG. 1

STATIC NUCLEAR POLARIZATION. BRUTE FORCE METHOD. $\gamma_n > 0$. NUCLEAR ZEEMAN ENERGY >> HYPERFINE INTERACTION ENERGY.

$$\mathcal{E} = +1, \; P_N = +\frac{\delta}{2}, \; P_e = -\frac{\Delta}{2}.$$

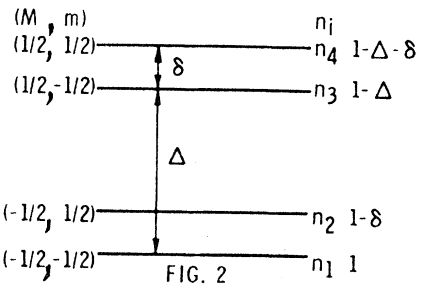

FIG. 2

STATIC NUCLEAR POLARIZATION. BRUTE FORCE METHOD. $\gamma_n < 0$. NUCLEAR ZEEMAN ENERGY >> HYPERFINE INTERACTION ENERGY.

$$\mathcal{E} = +1, \; P_N = -\frac{\delta}{2}, \; P_e = -\frac{\Delta}{2}.$$

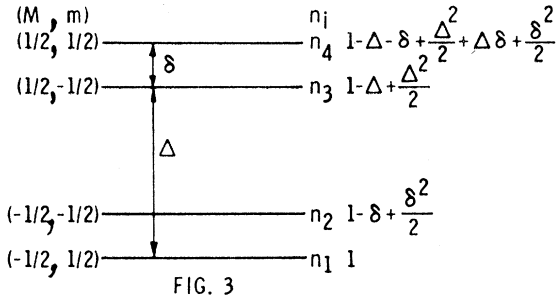

FIG. 3

STATIC NUCLEAR POLARIZATION. ROSE-GORTER METHOD. $A>0$. HYPERFINE INTERACTION ENERGY >> NUCLEAR ZEEMAN ENERGY.

$$\mathcal{E}=+1,\ P_N=+\frac{\Delta\delta}{4},\ P_e=-\frac{\Delta}{2}.$$

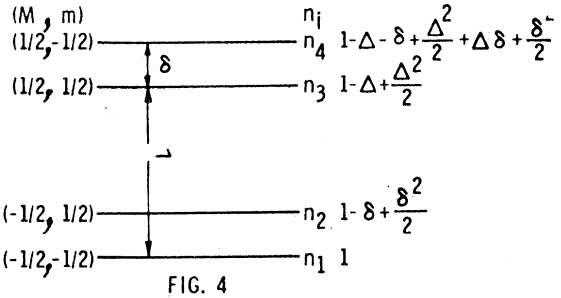

FIG. 4

STATIC NUCLEAR POLARIZATION. ROSE-GORTER METHOD. $A<0$. HYPERFINE INTERACTION ENERGY >> NUCLEAR ZEEMAN ENERGY.

$$\mathcal{E}=+1,\ P_N=-\frac{\Delta\delta}{4},\ P_e=-\frac{\Delta}{2}.$$

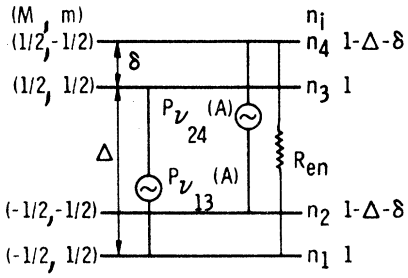

FIG. 5

DYNAMIC NUCLEAR POLARIZATION. OVERHAUSER EFFECT. $\gamma_n>0$. NUCLEAR ZEEMAN ENERGY >> HYPERFINE INTERACTION ENERGY. FLIP-FLOP RELAXATION DUE $\vec{I}\cdot\vec{S}$ COUPLING.

$$\mathcal{E}=+\frac{(\Delta+\delta)}{\delta},\ P_N=+\frac{(\Delta+\delta)}{2},\ P_e=0.$$

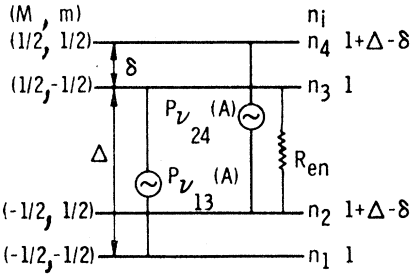

FIG. 6

DYNAMIC NUCLEAR POLARIZATION. OVERHAUSER EFFECT. $\gamma_n<0$. NUCLEAR ZEEMAN ENERGY >> HYPERFINE INTERACTION ENERGY. FLIP-FLOP RELAXATION DUE $\vec{I}\cdot\vec{S}$ COUPLING.

$$\mathcal{E}=-\frac{(\Delta-\delta)}{\delta},\ P_N=+\frac{(\Delta-\delta)}{2},\ P_e=0$$

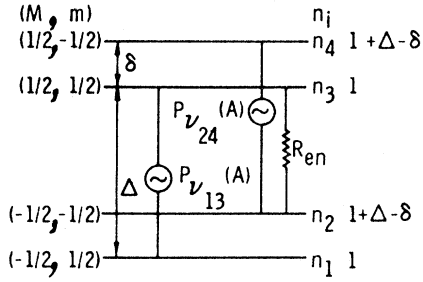

FIG. 7

DYNAMIC NUCLEAR POLARIZATION. OVERHAUSER EFFECT. $\gamma_n>0$. NUCLEAR ZEEMAN ENERGY >> HYPERFINE INTERACTION ENERGY. FLIP-FLIP RELAXATION DUE DIPOLAR COUPLING.

$$\mathcal{E}=-\frac{(\Delta-\delta)}{\delta},\ P_N=-\frac{(\Delta-\delta)}{2},\ P_e=0.$$

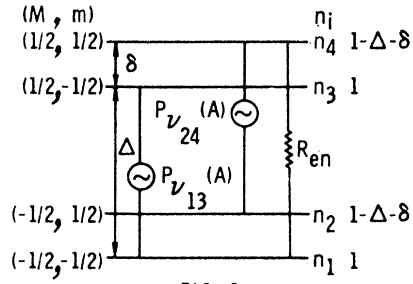

FIG. 8

DYNAMIC NUCLEAR POLARIZATION. OVERHAUSER EFFECT. $\gamma_n<0$. NUCLEAR ZEEMAN ENERGY >> HYPERFINE INTERACTION ENERGY. FLIP-FLIP RELAXATION DUE DIPOLAR COUPLING.

$$\mathcal{E}=+\frac{(\Delta+\delta)}{\delta},\ P_N=-\frac{(\Delta+\delta)}{2},\ P_e=0.$$

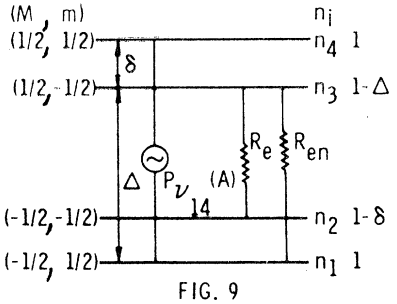

FIG. 9

DYNAMIC NUCLEAR POLARIZATION. OVERHAUSER EFFECT. A > 0. HYPERFINE INTERACTION ENERGY >> NUCLEAR ZEEMAN ENERGY. PARAMAGNETIC AND FLIP-FLOP RELAXATION.

$$\mathcal{E} = -\frac{(\Delta-\delta)}{2\delta}, \quad P_N = +\frac{(\Delta+\delta)}{4}, \quad P_e = -\frac{(\Delta-\delta)}{4}.$$

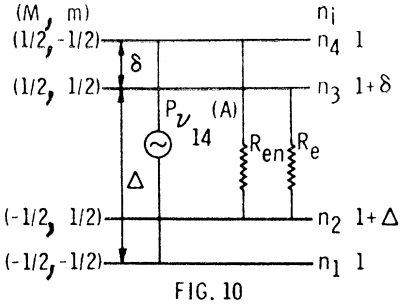

FIG. 10

DYNAMIC NUCLEAR POLARIZATION. OVERHAUSER EFFECT. A < 0. HYPERFINE INTERACTION ENERGY >> NUCLEAR ZEEMAN ENERGY. PARAMAGNETIC AND FLIP-FLOP RELAXATION.

$$\mathcal{E} = -\frac{(\Delta-\delta)}{2\delta}, \quad P_N = +\frac{(\Delta+\delta)}{4}, \quad P_e = -\frac{(\Delta-\delta)}{4}.$$

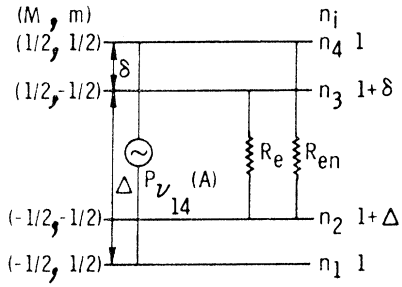

FIG. 11

DYNAMIC NUCLEAR POLARIZATION. OVERHAUSER EFFECT. A > 0. HYPERFINE INTERACTION ENERGY >> NUCLEAR ZEEMAN ENERGY. PARAMAGNETIC AND FLIP-FLIP RELAXATION.

$$\mathcal{E} = -\frac{(\Delta-\delta)}{2\delta}, \quad P_N = -\frac{(\Delta+\delta)}{4}, \quad P_e = -\frac{(\Delta-\delta)}{4}$$

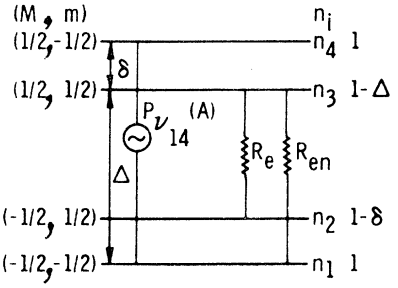

FIG. 12

DYNAMIC NUCLEAR POLARIZATION. OVERHAUSER EFFECT. A < 0. HYPERFINE INTERACTION ENERGY >> NUCLEAR ZEEMAN ENERGY. PARAMAGNETIC AND FLIP-FLIP RELAXATION.

$$\mathcal{E} = -\frac{(\Delta-\delta)}{2\delta}, \quad P_N = -\frac{(\Delta+\delta)}{4}, \quad P_e = -\frac{(\Delta-\delta)}{4}.$$

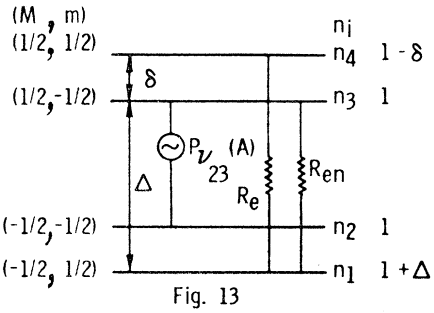

Fig. 13

DYNAMIC NUCLEAR POLARIZATION. OVERHAUSER EFFECT. A > 0. HYPERFINE INTERACTION ENERGY >> NUCLEAR ZEEMAN ENERGY. PARAMAGNETIC AND FLIP-FLOP RELAXATION.

$$\mathcal{E} = +\frac{(\Delta+\delta)}{2\delta}, \quad P_N = +\frac{(\Delta-\delta)}{4}, \quad P_e = -\frac{(\Delta+\delta)}{4}$$

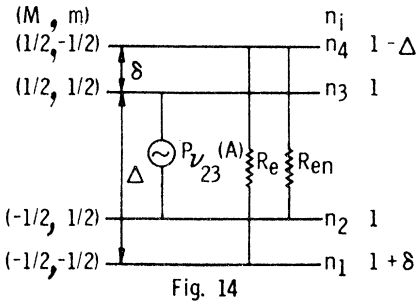

Fig. 14

DYNAMIC NUCLEAR POLARIZATION. OVERHAUSER EFFECT. A < 0. HYPERFINE INTERACTION ENERGY >> NUCLEAR ZEEMAN ENERGY. PARAMAGNETIC AND FLIP-FLOP RELAXATION.

$$\mathcal{E} = +\frac{(\Delta+\delta)}{2\delta}, \quad P_N = +\frac{(\Delta-\delta)}{4}, \quad P_e = -\frac{(\Delta+\delta)}{4}$$

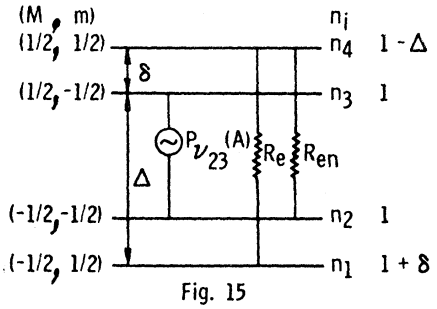

Fig. 15

DYNAMIC NUCLEAR POLARIZATION. OVERHAUSER EFFECT. A > 0. HYPERFINE INTERACTION ENERGY >> NUCLEAR ZEEMAN ENERGY. PARAMAGNETIC AND FLIP-FLIP RELAXATION.

$$\mathcal{E} = +\frac{(\Delta+\delta)}{2\delta},\ P_N = -\frac{(\Delta-\delta)}{4},\ P_e = -\frac{(\Delta+\delta)}{4}$$

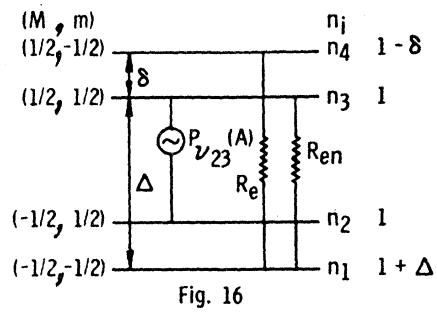

Fig. 16

DYNAMIC NUCLEAR POLARIZATION. OVERHAUSER EFFECT. A < 0. HYPERFINE INTERACTION ENERGY >> NUCLEAR ZEEMAN ENERGY. PARAMAGNETIC AND FLIP-FLIP RELAXATION.

$$\mathcal{E} = +\frac{(\Delta+\delta)}{2\delta},\ P_N = -\frac{(\Delta-\delta)}{4},\ P_e = -\frac{(\Delta+\delta)}{4}.$$

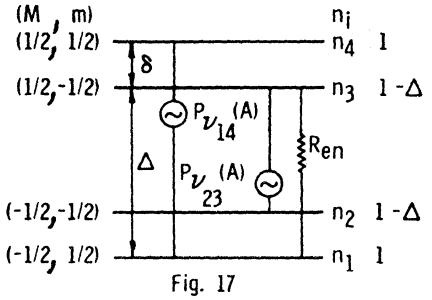

Fig. 17

DYNAMIC NUCLEAR POLARIZATION. OVERHAUSER EFFECT. A > 0. HYPERFINE INTERACTION ENERGY >> NUCLEAR ZEEMAN ENERGY. FLIP-FLOP RELAXATION.

$$\mathcal{E} = 0,\ P_N = +\frac{\Delta}{2},\ P_e = 0.$$

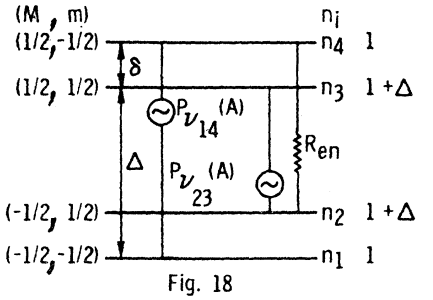

Fig. 18

DYNAMIC NUCLEAR POLARIZATION. OVERHAUSER EFFECT. A < 0. HYPERFINE INTERACTION ENERGY >> NUCLEAR ZEEMAN ENERGY. FLIP-FLOP RELAXATION.

$$\mathcal{E} = 0,\ P_N = +\frac{\Delta}{2},\ P_e = 0.$$

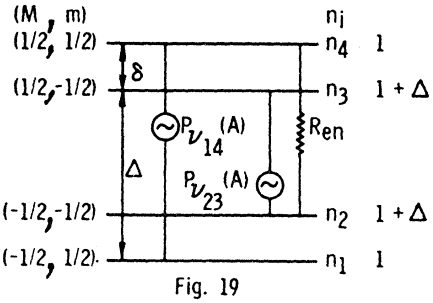

Fig. 19

DYNAMIC NUCLEAR POLARIZATION. OVERHAUSER EFFECT. A > 0. HYPERFINE INTERACTION ENERGY >> NUCLEAR ZEEMAN ENERGY. FLIP-FLIP RELAXATION.

$$\mathcal{E} = 0,\ P_N = -\frac{\Delta}{2},\ P_e = 0.$$

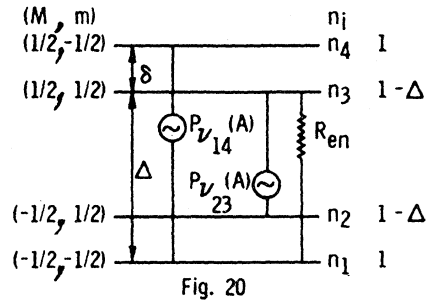

Fig. 20

DYNAMIC NUCLEAR POLARIZATION. OVERHAUSER EFFECT. A < 0. HYPERFINE INTERACTION ENERGY >> NUCLEAR ZEEMAN ENERGY. FLIP-FLIP RELAXATION.

$$\mathcal{E} = 0,\ P_N = -\frac{\Delta}{2},\ P_e = 0.$$

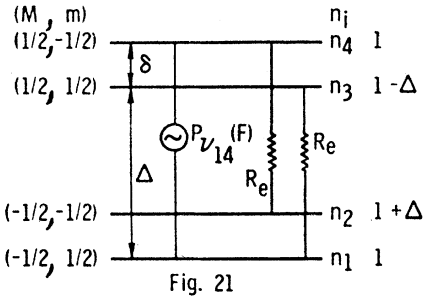

Fig. 21

DYNAMIC NUCLEAR POLARIZATION. JEFFRIES-ABRAGAM EFFECT. $\gamma_n > 0$. NUCLEAR ZEEMAN ENERGY >>HYPERFINE INTERACTION ENERGY. PARAMAGNETIC RELAXATION.

$$\mathcal{E} = -\frac{\Delta}{\delta},\ P_N = -\frac{\Delta}{2},\ P_e = -\frac{\Delta}{2}.$$

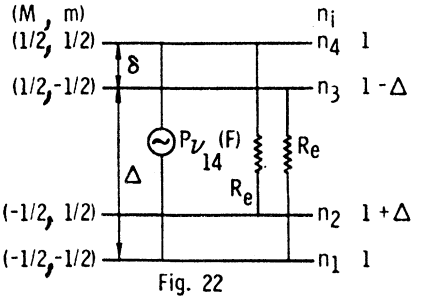

Fig. 22

DYNAMIC NUCLEAR POLARIZATION. JEFFRIES-ABRAGAM EFFECT. $\gamma_n < 0$. NUCLEAR ZEEMAN ENERGY >>HYPERFINE INTERACTION ENERGY. PARAMAGNETIC RELAXATION.

$$\mathcal{E} = -\frac{\Delta}{\delta},\ P_N = +\frac{\Delta}{2},\ P_e = -\frac{\Delta}{2}.$$

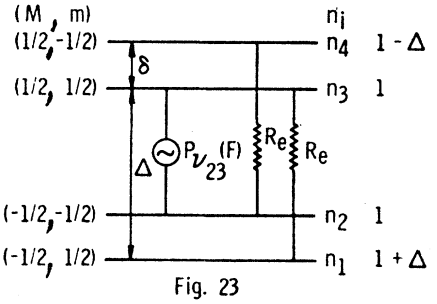

Fig. 23

DYNAMIC NUCLEAR POLARIZATION. JEFFRIES-ABRAGAM EFFECT. $\gamma_n > 0$. NUCLEAR ZEEMAN ENERGY >>HYPERFINE INTERACTION ENERGY. PARAMAGNETIC RELAXATION.

$$\mathcal{E} = +\frac{\Delta}{\delta},\ P_N = +\frac{\Delta}{2},\ P_e = -\frac{\Delta}{2}.$$

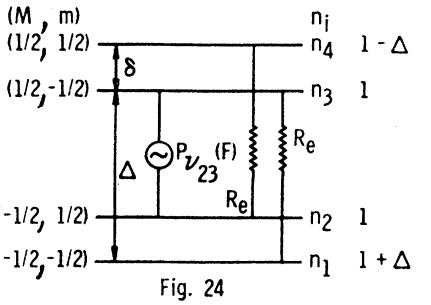

Fig. 24

DYNAMIC NUCLEAR POLARIZATION. JEFFRIES-ABRAGAM EFFECT. $\gamma_n < 0$. NUCLEAR ZEEMAN ENERGY >>HYPERFINE INTERACTION ENERGY. PARAMAGNETIC RELAXATION.

$$\mathcal{E} = +\frac{\Delta}{\delta},\ P_N = -\frac{\Delta}{2},\ P_e = -\frac{\Delta}{2}.$$

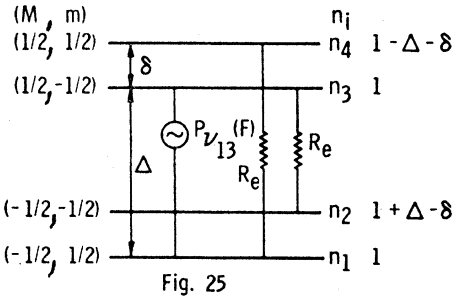

Fig. 25

DYNAMIC NUCLEAR POLARIZATION. JEFFRIES-ABRAGAM EFFECT. $A > 0$. HYPERFINE INTERACTION ENERGY >>NUCLEAR ZEEMAN ENERGY. PARAMAGNETIC RELAXATION.

$$\mathcal{E} = +1,\ P_N = -\frac{\Delta}{2},\ P_e = -\frac{\Delta}{2}.$$

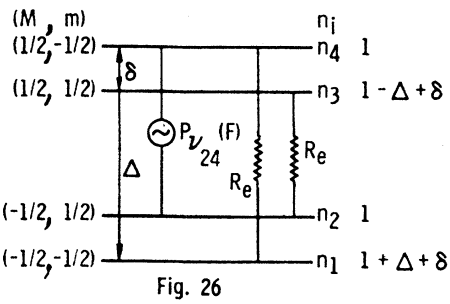

Fig. 26

DYNAMIC NUCLEAR POLARIZATION. JEFFRIES-ABRAGAM EFFECT. $A < 0$. HYPERFINE INTERACTION ENERGY >>NUCLEAR ZEEMAN ENERGY. PARAMAGNETIC RELAXATION.

$$\mathcal{E} = +1,\ P_N = -\frac{\Delta}{2},\ P_e = -\frac{\Delta}{2}.$$

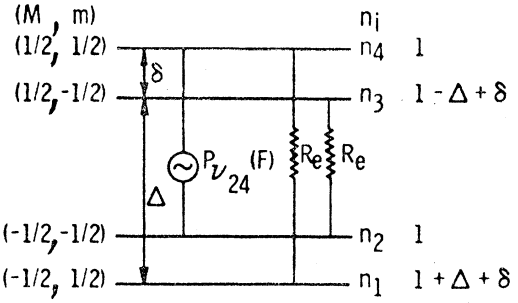

Fig. 27

DYNAMIC NUCLEAR POLARIZATION JEFFRIES-ABRAGAM EFFECT. A>0. HYPERFINE INTERACTION ENERGY >>NUCLEAR ZEEMAN ENERGY. PARAMAGNETIC RELAXATION.

$$\mathcal{E} = +1, \; P_N = +\frac{\Delta}{2}, \; P_e = -\frac{\Delta}{2}.$$

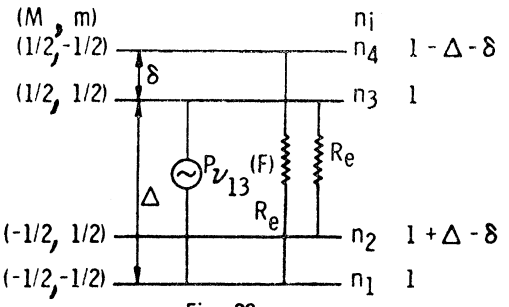

Fig. 28

DYNAMIC NUCLEAR POLARIZATION. JEFFRIES-ABRAGAM EFFECT. A<0. HYPERFINE INTERACTION ENERGY >>NUCLEAR ZEEMAN ENERGY. PARAMAGNETIC RELAXATION.

$$\mathcal{E} = +1, \; P_N = +\frac{\Delta}{2}, \; P_e = -\frac{\Delta}{2}.$$